New Journal of Physics
The open-access journal for physics

# Scaling the drop size in coflow experiments

**E Castro-Hernández[1], V Gundabala[2], A Fernández-Nieves[2] and J M Gordillo[1,3]**

[1] Área de Mecánica de Fluidos, Universidad de Sevilla, Avenida de los Descubrimientos s/n, 41092 Sevilla, Spain
[2] School of Physics, Georgia Institute of Technology, Atlanta, GA 30332, USA
E-mail: jgordill@us.es

*New Journal of Physics* **11** (2009) 075021 (17pp)
Received 9 February 2009
Published 31 July 2009
Online at http://www.njp.org/
doi:10.1088/1367-2630/11/7/075021

**Abstract.** We perform extensive experiments with coflowing liquids in microfluidic devices and provide a closed expression for the drop size as a function of measurable parameters in the jetting regime that accounts for the experimental observations; this expression works irrespective of how the jets are produced, providing a powerful design tool for this type of experiments.

**Contents**

**1. Introduction** **2**
**2. Experimental setup** **3**
**3. Experimental results and scaling** **4**
3.1. Revision of the narrowing regime . . . . . 4
3.2. Revisiting the dripping to jetting transition in the widening regime . . . . . 5
3.3. Unified scaling for the drop size . . . . . 7
**4. Conclusions** **13**
**Acknowledgments** **15**
**Appendix A. Solution of the generalized Tomotika's dispersion relation** **15**
**References** **16**

[3] Author to whom any correspondence should be addressed.

## 1. Introduction

The generation of emulsions is an area of active research due to its countless technological applications (see [1]–[5] for detailed reviews). Recent fabrication methods rely on microfluidics, as this technology provides great control over fluid flow and mixing of components. In many situations, the dispersed phase flows inside a coaxial coflow of the continuous phase; this provides several advantages with respect to using a quiescent bath [6]–[9]: (i) control of the drop size by appropriate tuning of the coflow properties; (ii) reduced coalescence between drops, in the absence of surfactants; and (iii) increased production frequency [10]–[17].

There are two major types of microfluidic devices that improve the drop or bubble generation process by making use of an outer, coaxial coflow: (i) those in which both streams flow through a small orifice, referred to as flow-focusing devices [15], [18]–[20] and (ii) those in which both streams flow in parallel, typically referred to as coflowing devices [10]–[14], [21]. The latter can also be classified in terms of the confinement provided by the outer bounding channel; there are situations where this confinement is significant [16, 22, 23], and situations where it is not [14, 21, 24, 25]. Despite these differences, the focus of all these studies is on understanding the transition between the dripping and the jetting regimes [26]–[28]. Dripping is characterized by the fact that no long jets of the dispersed phase are formed. Thus, drops are generated right at the tip of the injection tube. By contrast, when jetting occurs, the dispersed phase forms long liquid jets and consequently, drops are emitted right at the tip of the liquid thread.

In the absence of confinement effects, two different types of jetting regimes have been identified [21]: the *narrowing* and *widening* regimes. These names simply reflect the shape adopted by the jet in either regime. The narrowing jets are formed when the viscous stresses on the interface due to the outer stream overcome surface tension confinement forces, or equivalently, when the capillary number based on the outer velocity, $U_o = Q_o/D_o^2$, and outer viscosity, $\mu_o$, is $Ca_o = \mu_o U_o/\sigma \gtrsim O(1)$, with $\sigma$ the interfacial tension between the two liquids. Since in these situations, the outer velocity is larger than the inner velocity, the jet *stretches*, thus narrowing downstream by a certain amount. The widening jets are produced in a different way; they result when the stresses due to the flow of the inner stream at the interface overcome surface tension confinement forces. This can happen when the Weber number of the inner fluid satisfies the condition: $We_i = 8\rho_i Q_i^2/(\pi^2\sigma D_i^3) \gtrsim 1$, with $Q_i$ and $\rho_i$ the inner-fluid flow rate and density, respectively, and $D_i$ the inner diameter of the injection tube. In this situation, the inner stream usually flows faster than the outer stream; consequently, these jets are decelerated as they move downstream, resulting in their widened shape.

In this paper, we extend the criterion needed to induce the formation of a widening jet and show that the condition $We_i > 1$ is only applicable if the Reynolds number of the inner fluid, $Re_i$, is also larger than one. In the opposite limit, when $Re_i < 1$, the Weber number no longer reflects when a jet is formed. In this case, we find that the appropriate criterion is provided by the capillary number of the inner fluid; jetting occurs when $Ca_i > 1$. More importantly, we provide here a general expression to estimate the drop size in either regime as a function of measurable parameters; this shows that despite the differences between these regimes, the drop size is governed by a unique scaling relationship. Our experiments confirm this prediction, which can thus be used to design coflow experiments aimed at obtaining droplets with a particular size distribution. This capability coupled to the possibility of multiplexing [29] could contribute to the widespread use of this methodology.

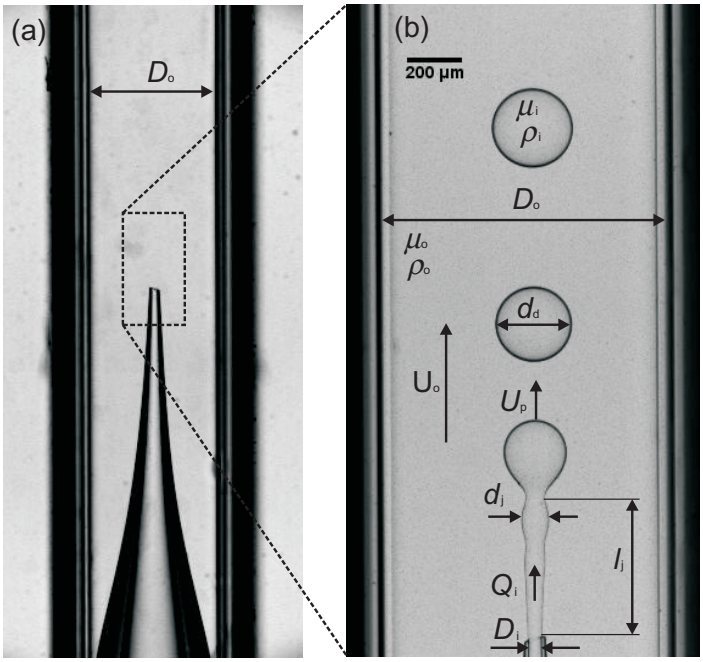


**Figure 1.** (a) Close up view of the tapered portion of the injection tube. Note that the untapered portion adjusts to the inner side of the outer squared capillary tube. (b) Coflowing device operated in the *widening regime* [21], characterized by a long liquid jet growing in diameter downstream of the injection tube. The definitions of the different variables used in the text are also indicated here.

The rest of the paper is structured as follows. The experimental setup is described in section 2. Section 3 is devoted to the analysis of the experimental results; we review the scaling of the drop size in the *narrowing* regime, provide the need to extend the current criterion to induce the formation of a widening jet, and derive and experimentally validate a simple equation to calculate the drop size in both *narrowing* and *widening* regimes. Finally, we conclude in section 4.

## 2. Experimental setup

Our experimental device is made of two coaxially aligned capillary tubes, as shown in figure 1. The inner capillary tube is cylindrical, with a tip tapered to an inner diameter $D_i$ that is varied between 40 and 60 $\mu$m and an outer diameter of approximately 80 $\mu$m. The outer capillary tube has a square cross section; coaxial alignment of the tubes is achieved by matching the outer diameter of the untapered portion of the inner capillary to the inner dimension of the square capillary, $D_o = 1$ mm, as shown in figure 1(a). At this length scale, which is below the capillary length, the effects of gravity are negligible. Therefore, the orientation of the experimental device with respect to that of gravity is irrelevant. Nonetheless, all experiments were aligned horizontally. Although the flow in the square tube is not axisymmetric, since the tip is centered and $D_i \ll D_o$, the local flow around the tip should be approximately axisymmetric. Both liquids are injected through syringe pumps (Harvard Apparatus PHD2000). For visualization and measurement purposes, we use a high-speed video camera Phantom V7.1, working between 2000 and 51 000 fps.

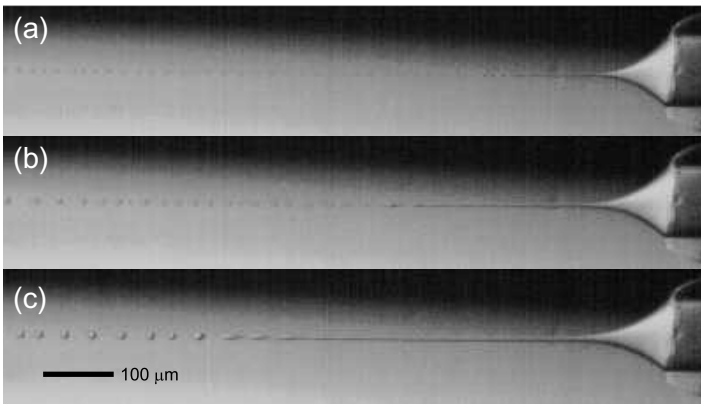


**Figure 2.** Example of the *stretching regime* [21], characterized by the ejection of a liquid jet with a diameter decreasing downstream. In the case illustrated in this figure, which shows a cone-jet transition, the coflowing device is operated under the tip-streaming regime, firstly described numerically by Suryo and Basaran [16]. The outer capillary number is $Ca_o = 4.32$, $Q_i/(U_o D_i^2) < 3 \times 10^{-3}$ and the inner flow rate is decreased from bottom to top. Picture taken from Marin *et al* [29].

The liquids we employ are deionized water, glycerol and different polydimethylsiloxane (PDMS) oils, with viscosities varying between 1.5 and 100 cP; by interchanging the different liquids we can vary the viscosity ratio, $\mu_i/\mu_o$, from 0.1 to 20. The surface tension between the different liquids, $\sigma$, slightly varies around 40 mN m$^{-1}$.

## 3. Experimental results and scaling

### *3.1. Revision of the narrowing regime*

It is well established that when the capillary number of the outer fluid in a coflow experiment exceeds a threshold value of order unity, a long liquid jet emerges from the injection tube [21, 29]. If in addition, $Q_i/U_o D_i^2 \ll 1$, the diameter of the liquid jet is much smaller than that of the injection tube, as illustrated in figure 2. In this situation, drops with sizes down to one micron can be obtained [29].

Within this *narrowing* regime, if the inner-fluid flow rate is kept constant while $U_o$ increases, the diameter of the ejected jet decreases [21, 29]. This results from the low Reynolds numbers in these experiments, which guarantee the effective diffusion of momentum across the whole section of the jet. As a result, the inner-liquid and outer-liquid velocities become equal some distance downstream of the injection tube and the jet diameter simply results from

$$\frac{\pi d_j^2}{4} U_o = Q_i \rightarrow d_j = \left(\frac{4Q_i}{\pi U_o}\right)^{1/2}. \quad (1)$$

The thin jets observed in this *narrowing* regime are convectively unstable and consequently, the size of the drops obtained from their break-up, $d_d$, can be deduced from the mass balance: $\pi d_d^3/6 = \pi^2 d_j^3/4k^*$, with $k^*(\mu_i/\mu_o, Oh)$ the dimensionless wavenumber corresponding to the

maximum growth rate of sinusoidal capillary perturbations and $\pi d_j/k^*$ its corresponding wavelength. Here, $Oh = \mu_i/\sqrt{\rho_i \sigma\, d_j/2}$ is the Ohnesorge number based on the material properties of the inner fluid, expressing the relative importance of viscous and inertial timescales [30]. Since $k^*$ depends weakly on $Oh$ for relatively large values of this parameter, as shown in the appendix (figure 12), it is sensible to write $k^* = k_t^*(\mu_i/\mu_o)$, with $k_t^*$ the wavenumber of maximum growth rate in the limit, firstly considered by Tomotika [31], of $Oh \to \infty$. With these considerations, we obtain

$$d_d = \left(\frac{144}{\pi}\right)^{1/6} (k_t^*)^{-1/3} \left(\frac{Q_i}{U_o}\right)^{1/2}, \tag{2}$$

which has been confirmed experimentally for a wide range of viscosity ratios [29].

This equation can be obtained using an alternative way of reasoning. Indeed, the drop volume can be obtained from the mass balance

$$\frac{\pi}{6} d_d^3 = Q_i f^{-1} = Q_i T, \tag{3}$$

with $f$ the drop formation frequency and $T$ the corresponding period. We can approximate the period of drop formation by the time needed to elongate the jet a distance equal to the wavelength of maximum growth rate, $T = \pi d_j/(k^* U_p)$, where $U_p$ is the velocity of the jet at its most downstream position, as shown in figure 1(b). By combining this result with equation (3), we obtain [21, 29]

$$\frac{\pi}{6} d_d^3 = Q_i \frac{\pi d_j}{k^* U_p} \to \frac{d_d}{D_i} = \frac{1}{D_i} \left(\frac{6 Q_i d_j}{k^* U_p}\right)^{1/3}. \tag{4}$$

Since $U_p = U_o$ for the *narrowing* jets considered so far, this equation (4) is identical to equation (2).

### 3.2. Revisiting the dripping to jetting transition in the widening regime

A different kind of jet, referred to as *widening* jet [21], is obtained if the inner momentum overcomes surface tension confinement forces: $We_i \gtrsim O(1)$. Generally, for these jets, $U_o \ll Q_i/D_i^2$ and thus, the jet is decelerated by the action of the shear stress exerted by the outer stream, leading to the observed jet widening, as shown in figure 1(b). We emphasize here that the condition for formation of these jets, $We_i = 8\rho_i Q_i^2/(\pi^2 \sigma D_i^3) \gtrsim 1$, only applies when, in addition, $Re_i = 2\rho_i Q_i/(\pi \mu_i D_i) \gtrsim 1$. If this is not fulfilled, the condition $We_i \gtrsim O(1)$ no longer predicts the dripping-to-jetting transition, as shown in figure 3(a), where we plot the values of the Weber number of the inner fluid for which we observe a jetting behavior; even for $We_i < 1$, there are jets that form. In these cases, $Re_i < 1$, as shown in figure 3(b). Interestingly, for these jets, the capillary number of the inner fluid is larger than one, $Ca_i = 4\mu_i Q_i/(\pi D_i^2 \sigma) \gtrsim 1$. We thus divide our data into two sets depending on whether the inner Reynolds number is smaller or larger than one. When $Re_i > 1$, we observe jetting if $We_i > 1$, as shown in figure 4(a). However, when $Re_i < 1$, widening jets form when $Ca_i > 1$, as shown in figure 4(b). As a result, widening jets can form either driven by inertial or viscous forces of the inner fluid; depending on $Re_i$, they form when either $We_i$ or $Ca_i$ is larger than a threshold number, which is close to unity. Our results thus extend the dripping-to-jetting criteria [21] to cases where $Re_i < 1$.

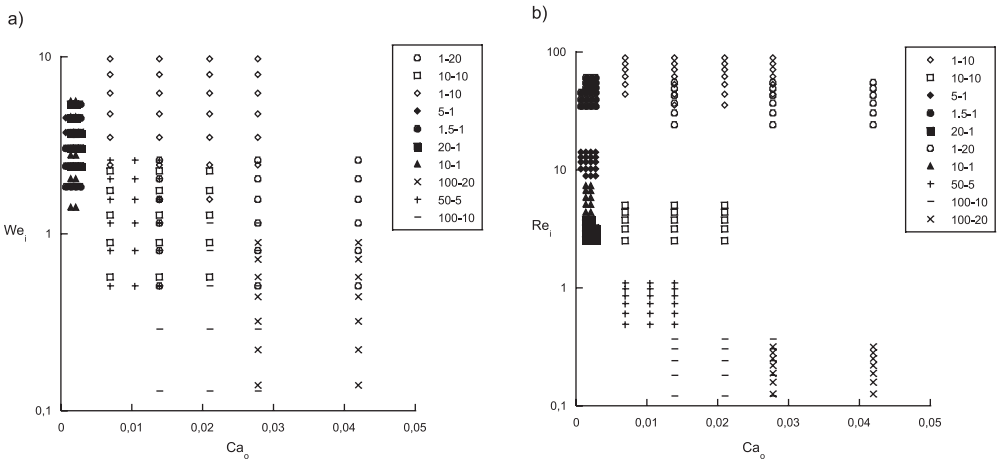


**Figure 3.** (a) Values of the Weber number evaluated at the exit of the injection tube, $We_\mathrm{i} = 8\rho_\mathrm{i} Q_\mathrm{i}^2/(\pi^2\sigma D_\mathrm{i}^3)$. All the experiments considered in this study lie within the widening regime [21] in spite some of the values of $We_\mathrm{i}$ are much smaller than unity. (b) Values of the inner Reynolds number, $Re_\mathrm{i} = 2\rho_\mathrm{i} Q_\mathrm{i}/(\pi\mu_\mathrm{i} D_\mathrm{i})$, at the exit of the injection tube. Numbers in the legend indicate inner/outer viscosities in centipoise.

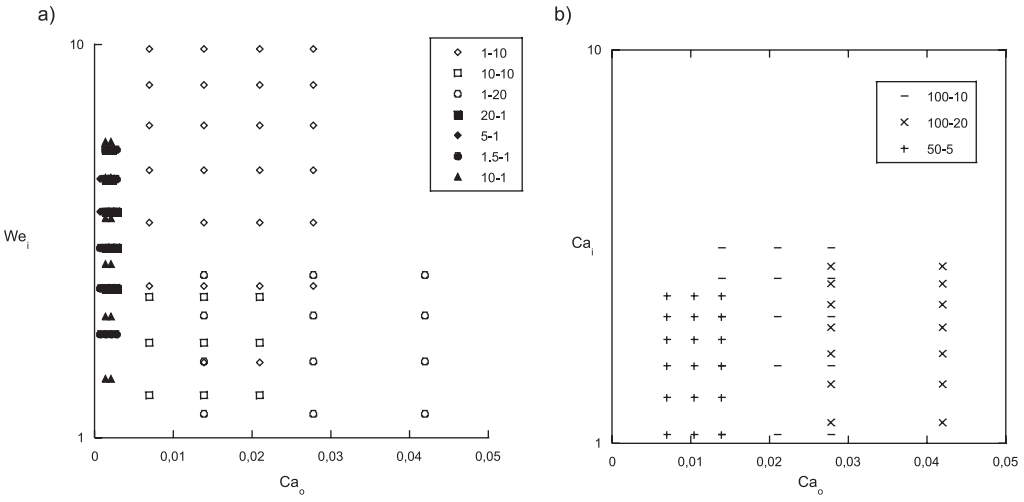


**Figure 4.** (a) Values of the Weber number evaluated at the exit of the injection tube, $We_\mathrm{i}$ for those experiments in which $Re_\mathrm{i} > 1$. (b) Values of the inner capillary number evaluated at the exit of the injection tube, $Ca_\mathrm{i} = 4\mu_\mathrm{i} Q_\mathrm{i}/(\pi D_\mathrm{i}^2\sigma)$ for those experiments in which $Re_\mathrm{i} < 1$. Thus, in order for widening jets to be generated, either $We_\mathrm{i} \gtrsim 1$ and $Re_\mathrm{i} \gtrsim 1$ or $Ca_\mathrm{i} \gtrsim 1$ and $Re_\mathrm{i} \lesssim 1$. Numbers in the legend indicate inner/outer viscosities in centipoise.

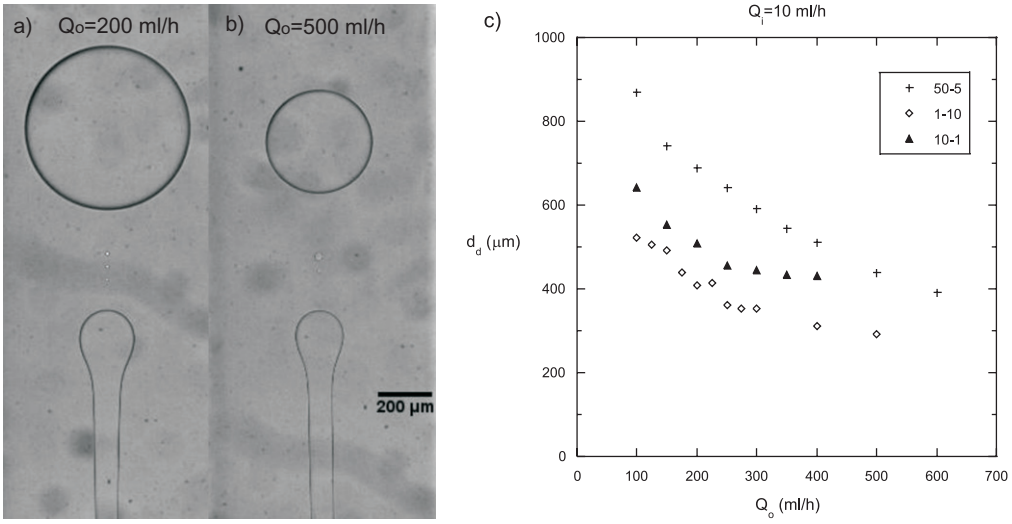


**Figure 5.** (a) and (b) These pictures illustrate the effect of increasing the outer flow rate while keeping constant the inner flow rate, $Q_\mathrm{i} = 10\,\mathrm{ml\,h^{-1}}$. The outer flow rate increases from left ($Q_\mathrm{o} = U_\mathrm{o} D_\mathrm{o}^2 = 200\,\mathrm{ml\,h^{-1}}$) to right ($Q_\mathrm{o} = U_\mathrm{o} D_\mathrm{o}^2 = 500\,\mathrm{ml\,h^{-1}}$). The values of the outer and inner viscosities are, respectively, $\mu_\mathrm{o} = 5\,\mathrm{cP}$ and $\mu_\mathrm{i} = 50\,\mathrm{cP}$. (c) Drop size as a function of the outer flow rate for a fixed value of the inner flow rate, $Q_\mathrm{i} = 10\,\mathrm{ml\,h^{-1}}$ and various inner/outer viscosities. Observe that the effect of increasing the outer flow rate is, in all cases, to decrease drop size.

### *3.3. Unified scaling for the drop size*

In the widening-jet regime, we observe that the drop diameter decreases as the coflow velocity increases, as shown in figures 5(a) and (b). This trend is consistent with what has been observed previously for both the narrowing and widening regimes [21, 29], and independent of the values of the inner and outer viscosities, as shown in figure 5(c).

We also observe that the drop size increases with the inner-fluid flow rate, for $\mu_\mathrm{i} = 1\,\mathrm{cP}$ and $\mu_\mathrm{o} = 10\,\mathrm{cP}$, as shown by the images in figure 6, which correspond to two different values of $Q_\mathrm{i}$; this is consistent with previous results too [21]. However, when $\mu_\mathrm{i} = 10\,\mathrm{cP}$ and $\mu_\mathrm{o} = 1\,\mathrm{cP}$, we observe that the drop size is reduced if $Q_\mathrm{i}$ is increased, as shown by the images in figure 7, which correspond to two different values of $Q_\mathrm{i}$. The viscosities of both inner and outer liquids thus play a relevant role in determining the drop-size dependence with $Q_\mathrm{i}$. Our experiments indicate that $d_\mathrm{d}$ increases with $Q_\mathrm{i}$ when the outer viscosity is sufficiently larger than that of water, irrespective of the viscosity ratio, as shown in figure 7(c), where we show data corresponding to $\mu_\mathrm{i}/\mu_\mathrm{o} = 0.1$, 1 and 10, all exhibiting the same behavior. By contrast, when the viscosity of the outer fluid is $\sim 1\,\mathrm{cP}$, the drop size decreases with $Q_\mathrm{i}$, as also shown in figure 7(c).

To understand these observations, let us consider the drop formation period in equation (3). Similarly to bubble formation, this time corresponds to the time required to convect the inner fluid a distance $\lambda$ at a velocity $U_\mathrm{p}$, $t_\mathrm{conv} = \lambda / U_\mathrm{p}$, plus the time required to collapse or pinch the liquid thread, $t_\mathrm{pinch}$: $T = t_\mathrm{conv} + t_\mathrm{pinch}$ [17], where $\lambda$ is taken as the distance traveled by the downstream location of the jet within two consecutive pinch-off events, as shown in figure 8.

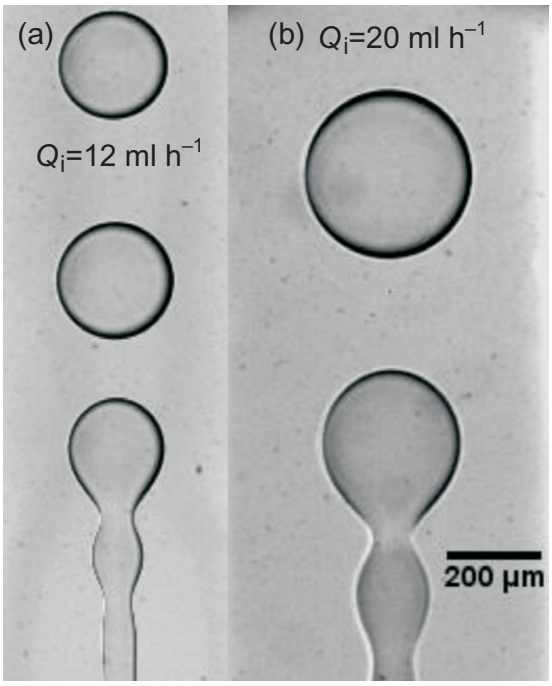


**Figure 6.** (a) and (b) These pictures illustrate the effect of increasing $Q_i$ while keeping the outer flow rate constant ($Q_o = 400\,\mathrm{ml\,h^{-1}}$). The inner flow rate increases from left ($Q_i = 12\,\mathrm{ml\,h^{-1}}$) to right ($Q_i = 20\,\mathrm{ml\,h^{-1}}$). The values of the outer and inner viscosities are, respectively, $\mu_o = 10\,\mathrm{cP}$ and $\mu_i = 1\,\mathrm{cP}$.

The pinch-off time depends on the Ohnesorge number. For $Oh \ll 1$, it is of the order of the capillary time, $t_{\mathrm{pinch}} \sim t_c = (\rho_i D_i^3/\sigma)^{1/2}$, while for $Oh \gtrsim O(1)$, it is of the order of the viscous diffusion time, $t_{\mathrm{pinch}} \sim t_{\mathrm{visc}} = \mu_i D_i/\sigma$. Therefore, either

$$T \sim \frac{\lambda}{U_p}\left(1 + \frac{D_i}{\lambda}\left(\frac{\rho_i U_p^2 D_i}{\sigma}\right)^{1/2}\right), \quad \text{if} \quad Oh \ll 1, \tag{5}$$

or

$$T \sim \frac{\lambda}{U_p}\left(1 + \frac{D_i}{\lambda}\left(\frac{\mu_i U_p}{\sigma}\right)\right), \quad \text{if} \quad Oh \gtrsim O(1). \tag{6}$$

In our experiments, the second term in the right-hand side of these equations is much smaller than unity. This implies that irrespective of the Ohnesorge number, the process of extending the liquid ligament a distance $\lambda$ is much slower than the break-up time of the liquid thread:

$$t_{\mathrm{conv}} \gg t_{\mathrm{pinch}} \implies f \propto U_p/\lambda. \tag{7}$$

The scaling of $d_d$ thus depends on how $\lambda$ and $U_p$ scale with the different control parameters in the problem. For $U_p$, when the outer fluid viscosity is large compared to that of water, we find that $U_p \simeq U_o$, as shown in figures 9(a) and (b), where we plot $U_p/U_o$ versus $Q_i$ and $Q_o$, respectively. As a result, $f \propto \lambda/U_o$, as in the case of bubble formation in the presence of a liquid coflow [13, 17] or for the case of drop formation in the narrowing regime [21, 29]. However,

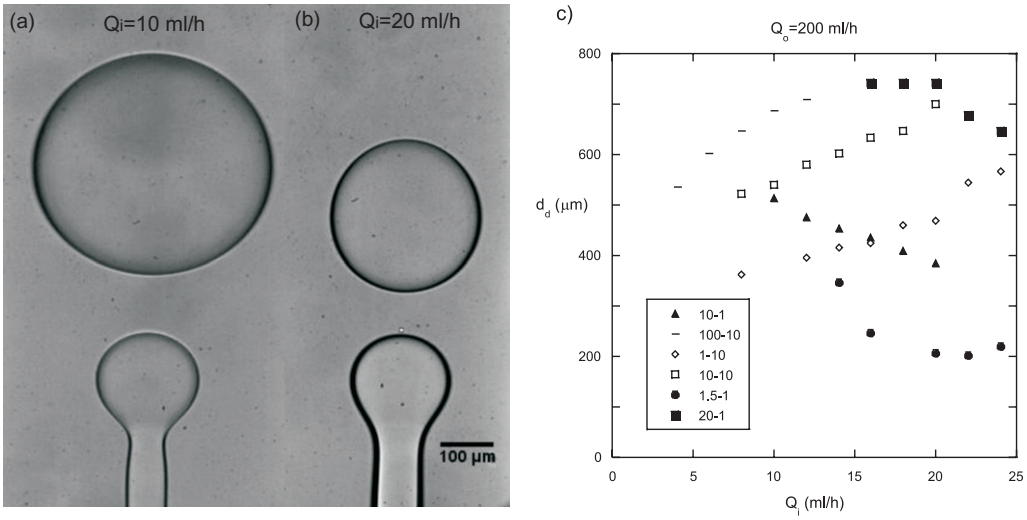


**Figure 7.** (a) and (b) These pictures illustrate the effect of increasing $Q_i$ ($Q_i = 10\,\mathrm{ml\,h^{-1}}$ in (a) and $Q_i = 20\,\mathrm{ml\,h^{-1}}$ in (b)) while keeping the outer flow rate constant ($Q_o = 300\,\mathrm{ml\,h^{-1}}$). $\mu_o = 1\,\mathrm{cP}$ and $\mu_i = 10\,\mathrm{cP}$. Contrary to the case depicted in figure 6, drop size decreases when the inner flow rate is increased. (c) Dependence of drop diameter on $Q_i$ for a fixed value of $Q_o$ and various inner/outer viscosities. Observe that the trends are different depending on the values of the inner and outer viscosities. Numbers in the legend indicate inner/outer viscosities in centipoise.

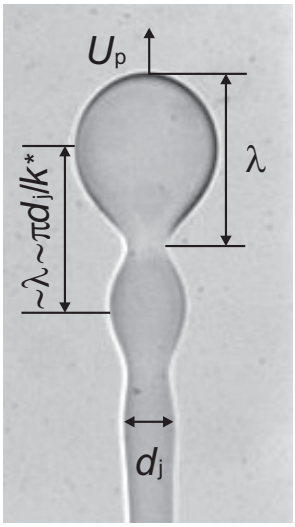


**Figure 8.** Picture showing the definition of $d_j$, jet diameter at the location where drops are emitted, and $\lambda$, axial distance traveled by the tip of the jet from two consecutive pinch-off events. As discussed in the text, the value of $\lambda$ can approach the wavelength of the maximum growth rate of capillary perturbations, $\pi d_j / k^*$.

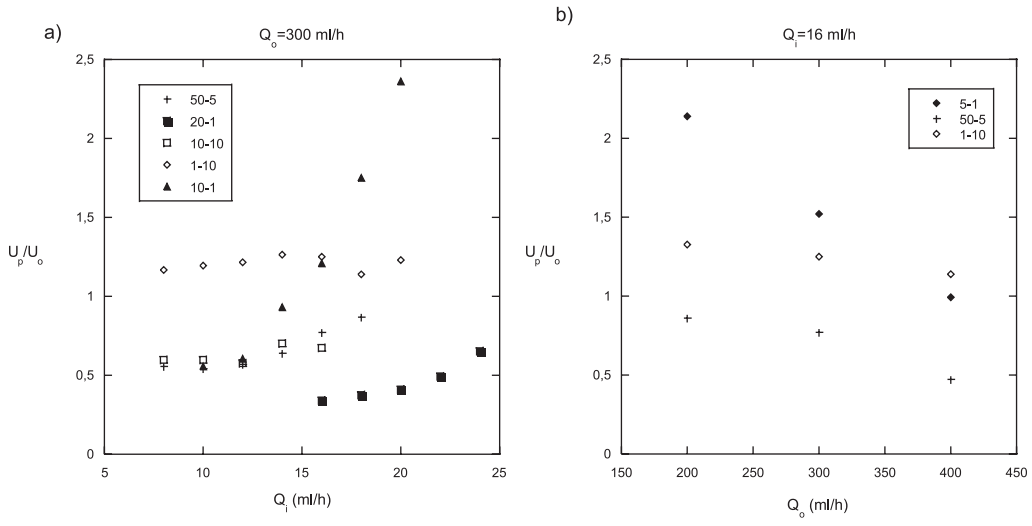


**Figure 9.** Ratio $U_p/U_o$, with $U_p$ the velocity at the tip of the drop (see figure 1) as a function of $Q_i$ and $Q_o$ for various inner/outer viscosities. See the discussion in the main body of the text.

when the outer viscosity is similar to that of water, $U_p$ exhibits dependence on both $U_o$ and $Q_i$, as shown in figure 9. This experimental observation can be qualitatively explained in terms of the viscous–stress balance on the jet surface. If we assume that the jet surface travels at a speed $U_s$, the continuity of shear stresses at the interface demands that $\mu_i\,(U_i - U_s)/D_i \sim \mu_o(U_s - U_o)/\delta$, with $U_i = 4Q_i/(\pi D_i^2)$ the average inner-fluid velocity and $\delta \sim D_i\sqrt{\mu_o/(\rho_o U_s D_i)}$ the thickness of the shear layer, which we schematically represent in figure 10. From this last equation, we obtain an estimate for $U_s$:

$$U_s \sim \frac{U_o + (\mu_i/\mu_o) \times (\delta/D_i)\, U_i}{1 + (\mu_i/\mu_o) \times (\delta/D_i)}. \tag{8}$$

Based on this equation, we see that in the limit $(\mu_i/\mu_o) \times (\delta/D_i) \ll 1$, $U_s \simeq U_o$ and consequently, $U_p \simeq U_o$, since in this case the differences between the interfacial and outer velocities are negligible. However, when the outer-fluid viscosity is not so large, then $(\mu_i/\mu_o) \times (\delta/D_i) \gtrsim O(1)$ and, due to the fact that $U_i \gg U_o$, $U_s \sim U_i[(\mu_i/\mu_o) \times (\delta/D_i) + U_o/U_i]/[1 + (\mu_i/\mu_o) \times (\delta/D_i)] \gtrsim O(U_o)$. Under these circumstances, the inner stream *drags* the outer fluid creating a strong velocity gradient adjacent to the jet interface, as schematically shown in figure 10(b). Since the outer velocities in the neighborhood of the jet interface are larger than $U_o$, $U_p$ is also larger than $U_o$. As $Q_o$ increases, however, this difference decreases and $U_p$ approaches $U_o$, as shown in figure 9(b). In addition, since $U_s$ grows with $U_i$, so does $U_p$, also consistent with our observations, as shown in figure 9(a).

Despite this qualitative agreement with our model, we have not been able to find a simple way of expressing $U_p$ as a function of the control parameters, other than solving the Navier–Stokes equations, which would have to be done numerically. Under confinement [22], the presence of the outer walls attenuates the growth of capillary waves and both the inner and outer velocity profiles are able to reach the parallel Poiseuille solution, simplifying the problem. In our experiments, this is not the case and the larger growth rate of the capillary waves disrupts the jet before the velocity profiles reach this analytic solution. Therefore, the velocities of the

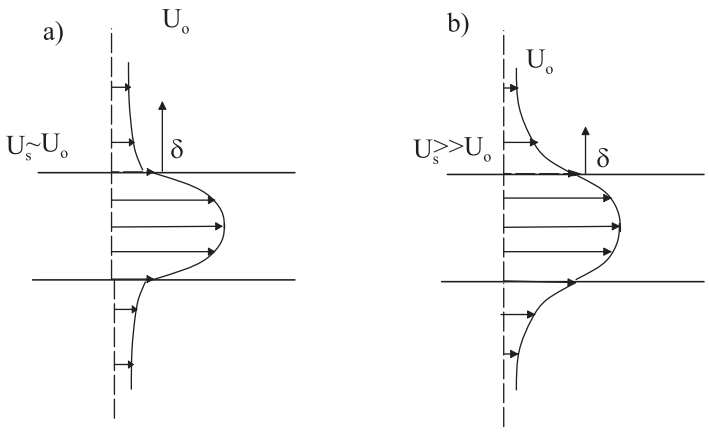


**Figure 10.** Sketch showing the effect of the shear exerted by the inner stream on the outer stream. Depending on the value of the outer viscosity, the interfacial velocities, $U_s$ are (a) similar to $U_o$ if $\mu_o \gg \mu_i$ or (b) considerably larger than $U_o$ if $\mu_i \gg \mu_o$.

inner and outer streams evolve in the axial direction in a nontrivial manner and so does the jet tip velocity $U_p$.

To obtain the appropriate scaling for $\lambda$, we take into account that the pinch-off process is driven by surface tension. Indeed, in order for surface tension to break a cylindrical piece of liquid into spherical drops, the wavelength of the growing, unstable mode, $\lambda_v$, must satisfy the condition $\lambda_v > \pi d_j$, with $d_j$ the jet diameter upstream the location where the drops form [32]–[34] (see figure 8). In addition, $t_{pinch} \ll t_{conv}$. As a result of these two ingredients, we can consider that right after a drop has been formed, the wavelength of the corrugations on the jet surface, shown in figure 8, is such that $k = \pi d_j/\lambda_v > 1$. Therefore, during the first instants of drop formation, surface tension smoothen all capillary waves. However, since the front of the jet is elongated at a velocity $U_p$, the wavelength of the corrugations increases in time and thus, $k$ decreases. When $k \simeq 1$, the liquid jet is close to being unstable and is prone to break into drops, however, the growth rates for $k \simeq 1$ are very small (see figure 11 for details)[4]. Consequently, $k$ continues to decrease in time until the growth rate of capillary perturbations is significant, namely, until $k \simeq k^*$. Since $t_{pinch}$ is so short compared to $t_{conv}$, the pinch-off process only represents a small fraction of the period for drop formation, $T$, and breakup essentially takes place *instantaneously* as soon as $\lambda \simeq \pi d_j/k^*$. Therefore, the drop formation period can be approximated by the time needed to elongate the jet a distance equal to $\lambda = \pi d_j/k^*$. As a result:

$$f = \frac{U_p}{\lambda} = \frac{k^*(Oh, \mu_i/\mu_o)\, U_p}{\pi d_j}. \tag{9}$$

[4] The dimensionless wavenumber $k$ is continuously decreasing in time as a consequence of the elongation imposed by the outer coflow. The elongation process starts from a value $k > 1$, and, thus, during the instants in which the 'effective' wavenumber is close to 1, which is the limit of stable/unstable disturbances, it is expected that the neck connecting the drop and the jet experiences oscillations.

Since continuity demands that $\pi/6\, d_{\mathrm{d}}^3 = Q_{\mathrm{i}}\, f^{-1}$, the drop diameter is given by:

$$\frac{d_{\mathrm{d}}}{D_{\mathrm{i}}} = \frac{1}{D_{\mathrm{i}}}\left(\frac{6\, Q_{\mathrm{i}}\, d_{\mathrm{j}}}{k^*\, U_{\mathrm{p}}}\right)^{1/3}, \tag{10}$$

which is *the same* as equation (4) used to calculate the diameter of the drops generated in the narrowing regime. We thus arrive at the relevant conclusion that the drop size is given by the same equation either in the widening or narrowing regimes; the only difference resides in how $k^*$, $d_{\mathrm{j}}$ and $U_{\mathrm{p}}$ depend on the control parameters.

For the widening jets, the best approach to obtain $k^*$ would be to solve the dispersion relation corresponding to the capillary perturbations evolving in a geometry which is between a cylinder and a spherical droplet. Moreover, these capillary perturbations develop within coflowing streams with shear. Therefore, contrary to the simplified analysis in the appendix, which assumes that the geometry is cylindrical, that there is no relative motion between both streams and that perturbations decay at infinity in the radial direction, a rigorous dispersion relation describing wave evolution in the case of widening jets, should take into account all the real effects enumerated above. Nevertheless, this refinement in the calculation of $k^*$ would necessarily imply simplifications since, for instance, the precise geometry of the transition region between the jet and the drop is not known *a priori*. Thus, we adopt here the simplest approach and calculate $k^*$ through equation (A.1), which gives the dimensionless wavenumber corresponding to the maximum growth rate. Note that in the case of widening jets the values of $Oh$ are not too large and thus the simplification $k^* \simeq k_t^*$, assumed for the case of the narrowing jets, is not applicable, as shown in figure 12(a).

Finally, we need to estimate $d_{\mathrm{j}}$. While for the narrowing jets we can use equation (1), for the widening jets this is not possible, since the inner stream velocity never equals the outer stream velocity, $U_{\mathrm{o}}$. This results from the fact that for these jets, the flow is locally absolutely unstable [25, 34], implying that at some axial location, the speed of the capillary disturbances becomes similar to the speed at which they are convected downstream. Therefore, the jet breaks before the inner velocity of the jet can become equal to the outer-fluid velocity. Based on this fact, we will estimate the value of $d_{\mathrm{j}}$ from the condition $U_{\mathrm{i}} = d_{\mathrm{j}}/t_{\mathrm{pinch}}$, with $U_{\mathrm{i}} = 4Q_{\mathrm{i}}/(\pi d_{\mathrm{j}}^2)$ the (approximate) propagation velocity of capillary disturbances and with $d_{\mathrm{j}}/t_{\mathrm{pinch}}$ the characteristic velocity at which perturbations grow in time. By using that $t_{\mathrm{pinch}} = 1/(\mathrm{i}\, n^*)(\rho_{\mathrm{i}}/\mu_{\mathrm{i}})(d_{\mathrm{j}}/2)^2$ (see appendix), with $(\mathrm{i}n^*)$ the maximum value of the growth rate, and the definition of $Oh$, we arrive at:

$$\frac{Oh^{-2}}{\mathrm{i}n^*}\frac{\mu_{\mathrm{i}}\, d_{\mathrm{j}}}{2\sigma} = \frac{\pi d_{\mathrm{j}}^3}{4Q_{\mathrm{i}}}. \tag{11}$$

Note that equation (11) needs to be solved iteratively since $\mathrm{i}n^*$ is also a function of $d_{\mathrm{j}}$ through its dependence on $Oh$. This maximum growth rate depends on $Oh$, as shown in figure 12(b) for different viscosity ratios; it appreciably decreases as $Oh$ increases.

Equipped with the theoretical description of $k^*$, $U_{\mathrm{p}}$ and $d_{\mathrm{j}}$, we can critically test the drop size dependence predicted by equation (10). We thus plot the experimental dimensionless ratio $d_{\mathrm{d}}/D_{\mathrm{i}}$ as a function of $(6Q_{\mathrm{i}}\, d_{\mathrm{j}}/(D_{\mathrm{i}}^3\, k^*\, U_{\mathrm{p}}))^{1/3}$, as shown in figure 13(a), where we measure $U_{\mathrm{p}}$ directly from the experiments, and in figure 13(b), where we use $U_{\mathrm{p}} = U_{\mathrm{o}}$ when $\mu_{\mathrm{o}} \geqslant 5\,\mathrm{cP}$. Remarkably, when doing so, all the data collapses onto the same mastercurve, irrespective of whether $d_{\mathrm{d}}$ increased or decreased with $Q_{\mathrm{i}}$, and for a large number of $\mu_{\mathrm{i}}$ and $\mu_{\mathrm{o}}$ combinations. We obtain that the spread of the data is $\pm 25\%$ (figure 13(a)) and $\pm 35\%$ (figure 13(b)) with

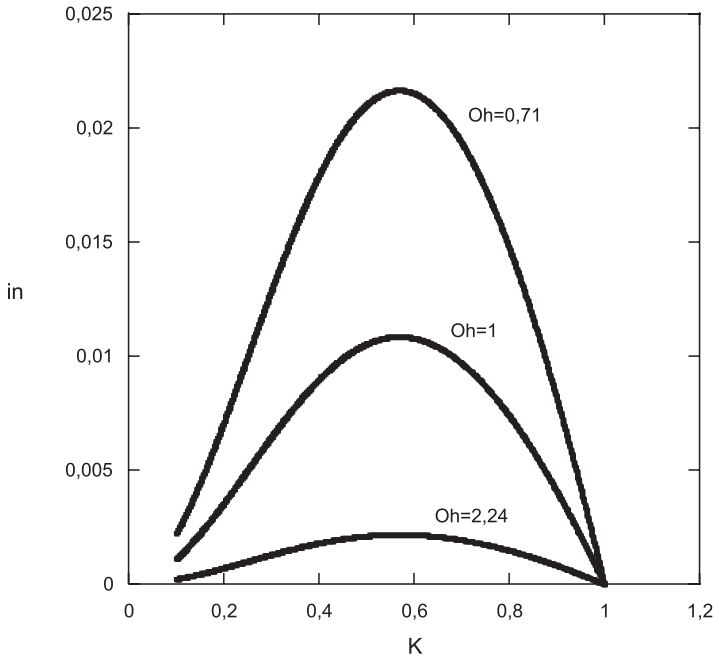


**Figure 11.** Dispersion relation curves for different values of the Ohnesorge number and values of the inner and outer viscosities $\mu_i = 1$ cP and $\mu_o = 10$ cP. Note that the wavelength of maximum amplification of capillary disturbances, $k^*$, varies very slightly with $Oh$. Moreover, note that perturbations with wavenumbers $k \simeq 1$, possess growth rates close to zero.

respect to the mean. In addition, there is a linear relation between these variables, consistent with our expectations. By performing a linear fit of the data, we obtain:

$$\frac{d_d}{D_i} = 0.97 \frac{1}{D_i} \left( \frac{6 Q_i d_j}{k^* U_p} \right)^{1/3} - 0.22 \,, \tag{12}$$

$$\frac{d_d}{D_i} = 0.9 \frac{1}{D_i} \left( \frac{6 Q_i \, d_j}{k^* U_p} \right)^{1/3} + 0.75 \,, \tag{13}$$

for figures 13(a) and (b), respectively. The slopes of the linear fits are close to one and the ordinates are close to zero, in further agreement with equation (10).

In spite of the relative errors in figure 13, we have shown that equations (12) and (13) can be used to approximately predict the drop size, even for the largest values of $(6 Q_i \, d_j / (D_i^3 k^* U_p))^{1/3}$, which correspond to drop sizes that are close to the outer geometrical dimension of the device. As a result, our conceptual description of the drop formation mechanism in coflowing liquids is correct, unifying the so-called narrowing and widening regimes in terms of the drop size.

## 4. Conclusions

We have studied in detail the process of drop formation from long, widening jets, in microfluidic coflowing devices [21]. By changing the values of the control parameters, which include inner-fluid and outer-fluid viscosities and flow rates, we have extended the criterion for jetting to occur

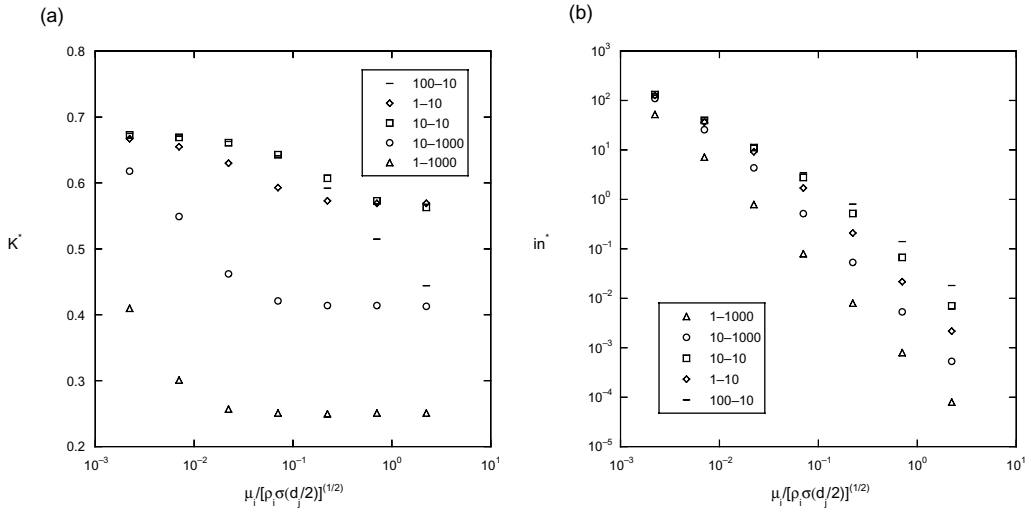


**Figure 12.** (a) Variation of the wavenumber of maximum growth rate $k^*$ as a function of the Ohnesorge number and for different values of the inner/outer viscosities. (b) Variation of the maximum growth rate $in^* = in(k^*)$ as a function of the Ohnesorge number and for different values of the inner/outer viscosities.

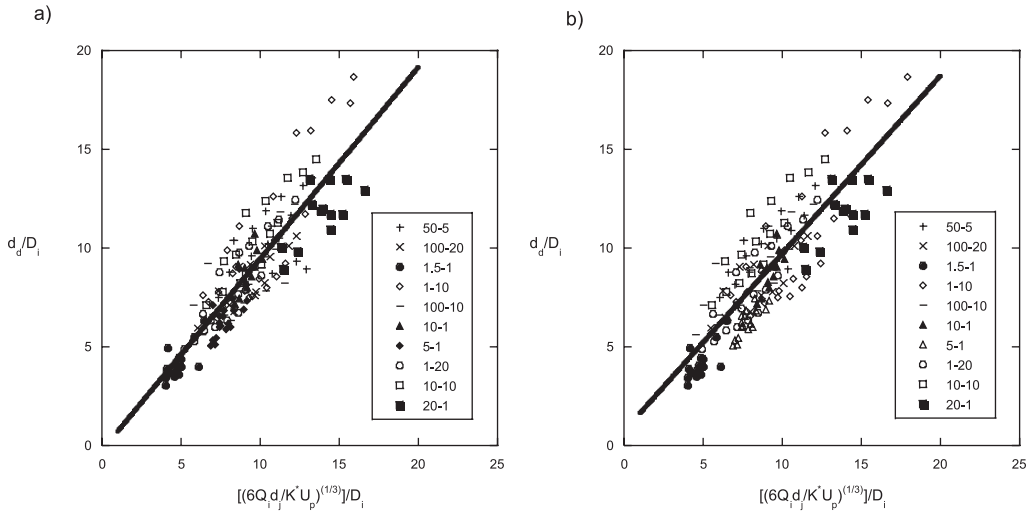


**Figure 13.** Experimentally measured drop diameters $d_\mathrm{d}/D_\mathrm{i}$ as a function of the parameter $(6Q_\mathrm{i}\, d_\mathrm{j}/(D_\mathrm{i}^3 k^* U_\mathrm{p}))^{1/3}$. In both graphs, the slope of the linear regression fit to the experimental data is very close to 1, which is the experimental prediction given in equation (10). The relative errors, however, are $\pm 30\%$. Since the maximum experimental error occurs in the measurement of the tip velocity but is only of the order of $\sim 10\%$, the dispersion is attributable to necessary simplifications in the way the wavelength of maximum growth rate and the tip velocity, $U_\mathrm{p}$, are calculated. Numbers in the legend indicate inner/outer viscosities in centipoise.

as a function of the Reynolds number of the inner fluid. When $Re_i > 1$, our results indicate that jetting occurs if $We_i > 1$, consistent with previous experiments [21], while for $Re_i < 1$, the correct measure to predict the transition from dripping to jetting is not $We_i$, but rather the capillary number of the inner fluid; jetting occurs in this case when $Ca_i > 1$.

By combining experiments and modeling, we have arrived at the conclusion that the physical idea underlying drop generation in both *narrowing* and the *widening* regimes [21] is the same: the period of drop formation is given by the time required to elongate the jet a distance equal to the wavelength of maximum growth rate. From a quantitative point of view, we have obtained that the size of the drops, $d_d$, generated either in the *narrowing* or in the *widening* jetting regimes can be calculated, with relative errors of about $\pm 30\%$, using a simple model relating $d_d$ to the dimensionless wavenumber corresponding to the maximum growth rate, $k^*$, to the jet diameter, $d_j$, and to the velocity of the most downstream point in the jet, $U_p$. As a result, the only difference between the drop size generated in either the narrowing or widening regimes is the way $k^*$, $d_j$ and $U_p$ depend on the control parameters.

For the narrowing jets, since the values of the Ohnesorge number are usually moderate or large, and due to the small variation of $k^*$ with $Oh$, we can approximate $k^*$ by $k_t^*$, which is the wavenumber corresponding to the maximum growth rate in the limit $Oh \to \infty$ considered by Tomotika [31]. For the widening jets, this simplification in the determination of $k^*$ is not applicable since the values of $Oh$ are not large enough.

Additionally, in the case of the *narrowing* jets, $d_j = (4Q_i/\pi D_i^2)^{1/2}$ and $U_p = U_o$, while for widening jets, $U_p = U_o \simeq Q_o/D_o^2$ only if the viscosity of the outer fluid is large enough; otherwise it needs to be determined experimentally. For these jets, we have obtained the value of $d_j$ by using the fact that these jets break-up through an absolute instability, implying that the relevant capillary velocity can be approximated by the inner-fluid, average velocity; using this fact and the approximate pinch-off time, we have estimated the jet diameter.

Our results provide a general description of the drop formation mechanism in coflowing liquids for both the narrowing and widening regimes through a unique relation for the drop size. This understanding can aid future experimental approaches to the generation of emulsions using coflowing devices.

## Acknowledgments

We thank financial support from the Spanish Ministry of Education under projects no. DPI2008-06624-C03-01,03. AF-N also thanks the University of Almeria.

## Appendix A. Solution of the generalized Tomotika's dispersion relation

Both the wavenumber of maximum growth rate $k^*$ and the maximum value of the growth rate $in^*$ of capillary sinusoidal perturbations of the form $e^{i\bar{n}t+\bar{k}z}$ propagating along a fluid cylinder which is surrounded by an infinite mass of another liquid, is reiteratively used in the main body of the paper. Thus, for clarity, we reproduce here the dispersion relation $F(in, k, Oh, \mu_i/\mu_o) = 0$, first

deduced by Tomotika [31] and first solved numerically by Meister and Scheele [30]:

$$\begin{vmatrix} I_1(k) & I_1(k_1) & K_1(k) & K_1(k_2) \\ kI_0(k) & k_1 I_0(k_1) & -kK_0(k) & -k_2 K_0(k_2) \\ 2(\mu_i/\mu_o)k^2 I_1(k) & (\mu_i/\mu_o)(k^2+k_1^2)I_1(k_1) & 2k^2 K_1(k) & (k^2+k_2^2)K_1(k_2) \\ F_1 & F_2 & F_3 & F_4 \end{vmatrix} = 0, \tag{A.1}$$

where

$$\bar{k} = kd_j/2, \tag{A.2}$$

$$Oh = \frac{\mu_i}{\sqrt{\rho_i \sigma d_j/2}}, \tag{A.3}$$

$$\bar{n} = \frac{\mu_i}{\rho_i (d_j/2)^2} n, \tag{A.4}$$

$$k_1 = \sqrt{k^2 + in}, \tag{A.5}$$

$$k_2 = \sqrt{k^2 + in\frac{\mu_i}{\mu_o}\frac{\rho_o}{\rho_i}}, \tag{A.6}$$

$$F_1 = ik^2 \frac{\mu_i}{\mu_o}[I_0(k) + I_2(k)] - n\frac{\mu_i}{\mu_o} I_0(k) + \frac{(k^2-1)k}{n\,Oh^2}\frac{\mu_i}{\mu_o} I_1(k), \tag{A.7}$$

$$F_2 = ik_1 k \frac{\mu_i}{\mu_o}[I_0(k_1) + I_2(k_1)] + \frac{(k^2-1)k}{n\,Oh^2}\frac{\mu_i}{\mu_o} I_1(k_1), \tag{A.8}$$

$$F_3 = -ik^2[K_0(k) + K_2(k)] + n\frac{\rho_o}{\rho_i}\frac{\mu_i}{\mu_o} K_0(k), \tag{A.9}$$

and

$$F_4 = -ik_2 k[K_0(k_2) + K_2(k_2)]. \tag{A.10}$$

Given a dimensionless wavenumber $k$, a viscosity ratio $\mu_i/\mu_o$, a density ratio $\rho_i/\rho_o \simeq 1$ and a value of the Ohnesorge number $Oh$, we have solved equation (A.1) using Mathematica.

## References


[1] Basaran O A 2002 Small-scale free surface flows with breakup: drop formation and emerging applications *AIChE J.* **48** 1842–8

[2] Squires T M and Quake S R 2005 Microfluidics: fluid physics at the nanoliter scale *Rev. Mod. Phys.* **77** 977–1026

[3] Stone H A, Stroock A D and Adjari A 2004 Engineering flows in small devices: microfluidics toward a lab-on-a-chip *Annu. Rev. Fluid Mech.* **36** 381–411

[4] Gunther A and Jensen K F 2006 Multiphase microfluidics: from flow characteristics to chemical and materials synthesis *Lab Chip* **6** 1487–503

[5] Barrero A and Loscertales I G 2007 Micro- and nanoparticles via capillary flows *Annu. Rev. Fluid Mech.* **39** 89–106

[6] Meister B J and Scheele G F 1969 Drop formation from cylindrical jets in immiscible liquid systems *AICHE J.* **15** 700–6

[7] Richards J R, Lenhoff A M and Beris A N 1994 Dynamic breakup of liquid–liquid jets *Phys. Fluids* **6** 2640–55
[8] Hommaa S, Kogaa J, Matsumotoa S, Songb M and Tryggvason G 2006 Breakup mode of an axisymmetric liquid jet injected into another immiscible liquid *Chem. Eng. Sci.* **61** 3986–96
[9] Webster D R and Longmire E K 2001 Jet pinch-off and drop formation in inmiscible liquid–liquid systems *Exp. Fluids* **30** 47–56
[10] Bragg L and Nye J F 1947 A dynamical model of a crystal structure *Proc. R. Soc.* A **190** 474–81
[11] Smith C S 1949 On blowing bubbles for bragg's dynamic crystal *J. Appl. Phys.* **20** 631
[12] Chuang S C and Goldschmidt V W 1970 Bubble formation due to a submerged capillary tube in quiescent and coflowing streams *Trans. ASME* D **92** 705–11
[13] Oguz H N and Prosperetti A 1993 Dynamics of bubble growth and detachment from a needle *J. Fluid Mech.* **257** 111–45
[14] Zhang D F and Stone H A 1997 Drop formation in viscous flows at a vertical capillary tube *Phys. Fluids* **9** 2234–42
[15] Ganan-Calvo A M and Gordillo J M 2001 Perfectly monodisperse microbubbling by capillary flow focusing *Phys. Rev. Lett.* **87** 274501
[16] Suryo R and Basaran O A 2006 Tip streaming from a liquid drop forming from a tube in a co-flowing outer fluid *Phys. Fluids* **18** 082102
[17] Gordillo J M, Sevilla A and Martínez-Bazán C 2007 Bubbling in a coflow at high Reynolds numbers *Phys. Fluids* **19** 077102
[18] Anna S L, Bontoux N and Stone H A 2003 Formation of dispersions using flow focusing in microchannels *Appl. Phys. Lett.* **82** 364–6
[19] Gordillo J M, Cheng Z, Márquez M, Gañán Calvo A M and Weitz D A 2004 A new device for the generation of microbubbles *Phys. Fluids* **16** 2828–34
[20] Garstecki P, Gitlin I, DiLuzio W, Whitesides G M, Kumacheva E and Stone H A 2004 Formation of monodisperse bubbles in a microfluidic flow-focusing device *Appl. Phys. Lett.* **85** 2649–51
[21] Utada A S, Fernández-Nieves A, Stone H A and Weitz D 2007 Dripping to jetting transitions in co-flowing liquid streams *Phys. Rev. Lett.* **99** 094502
[22] Guillot P, Colin A, Utada A S and Ajdari A 2007 Stability of a jet in confined pressure-driven biphasic flows at low Reynolds number *Phys. Rev. Lett.* **99** 104502
[23] Guillot P, Colin A and Ajdari A 2008 Stability of a jet in confined pressure-driven biphasic flows at low Reynolds number in various geometries *Phys. Rev.* E **78** 016307
[24] Ganan-Calvo A M and Riesco-Chueca P 2006 Jetting–dripping transition of a liquid jet in a lower viscosity co-flowing immiscible liquid: the minimum flow rate in flow focusing *J. Fluid Mech.* **553** 75–84
[25] Utada A S, Fernández-Nieves A, Gordillo J M and Weitz D 2008 Absolute instability of a liquid jet in a coflowing stream *Phys. Rev. Lett.* **100** 014502
[26] Clanet C and Lasheras J C 1999 Transition from dripping to jetting *J. Fluid Mech.* **383** 307–26
[27] Ambravaneswaran B, Subramani H J, Phillips S D and Basaran O A 2004 Dripping–jetting transitions in a dripping faucet *Phys. Rev. Lett.* **93** 034501
[28] Sevilla A, Gordillo J M and Martínez-Bazán C 2005 Transition from bubbling to jetting in a coaxial airwater jet *Phys. Fluids* **17** 018105
[29] Marin A G, Campo-Cortés F and Gordillo J M 2009 Generation of micron-sized drops and bubbles through viscous coflows *Colloids Surf.* A **344** 2–7
[30] Meister B J and Scheele G F 1967 Generalized solution of the tomotika stability analysis for a cylindrical jet *AIChE J.* **13** 682–6
[31] Tomotika S 1935 On the instability of a cylindrical thread of a viscous liquid surrounded by another viscous fluid *Proc. R. Soc.* A **150** 322–37
[32] Savart F 1833 Mémoire sur la constitution des veines liquides lancées par des orifices circulaires en mince paroi *Ann. Chim.* **53** 337–86
[33] Rayleigh W S 1978 On the instability of jets *Proc. London Math. Soc.* **10** 4–13
[34] Eggers J and Villermaux E 2008 Physics of liquid jets *Rep. Prog. Phys.* **71** 036601